J. Chem. Sci. Vol. 128, No. 8, August 2016, pp. 1211–1221.
DOI 10.1007/s12039-016-1118-9

Synthesis, molecular structure, spectroscopic investigations and computational study of a potential molecular switch of 2-([1,1'-biphenyl]-4-yl)-2-methyl-6-(4-nitrophenyl)-4-phenyl-1,3 diazabicyclo [3.1.0]hex-3-ene

AYOUB KANAANI, DAVOOD AJLOO*, HAMZEH KIYANI*, FRESHTE SHAHERI and MAJID AMIRI

School of Chemistry, Damghan University, Damghan, 36716-41167, Iran
e-mail: ajloo@du.ac.ir; hkiyani@du.ac.ir

MS received 29 December 2015; revised 9 April 2016; accepted 25 May 2016

Abstract. This work presents a combined experimental and theoretical study on a photochromic compound, 2-([1,1'-biphenyl]-4-yl)-2-methyl-6-(4-nitrophenyl)-4-phenyl-1,3 diazabicyclo [3.1.0]hex-3-ene, existing in closed form ('*A*') and open form ('*B*'). The spectroscopic properties of the title compound have been investigated by using IR, UV–Vis and ^{1}H NMR techniques. The molecular geometry and spectroscopic data of the title compound have been calculated by using the density functional method (B3LYP) invoking 6-311G(d,p) basis set. UV-Vis spectra of the two forms were recorded. The excitation energies, oscillator strength, etc., were calculated by time-dependent density functional theory (TD-DFT). Furthermore, molecular electrostatic potential map (MEP), frontier molecular orbital analysis (HOMO–LUMO), total density of state (TDOS) and reactivity descriptors were found and discussed. We applied a first-principles computational approach to study a light-sensitive molecular switch. We find that the conductance of the two isomers varies dramatically, which suggests that this system has potential use as a molecular switch.

Keywords. Photochromism; DFT; spectroscopy; molecular switch

1. Introduction

Photochromism is a phenomenon associated with reversible color and absorption spectral change of a molecule.[1] Photochromic compounds reversibly change geometrical structure.[2] Although many types of photochromic compounds have been reported, those exhibiting photochromism in solid state are very rare.[3] Depending on the special structure, 1,3-diazabicyclo[3.1.0]hex-3-ene derivative crystals show different colour such as blue, purple, yellow, purple, pink, brown, etc. with UV irradiation.[4,5] The photochromic behavior of "A" over "B" form can be assigned to the electron-withdrawing effect of *para*-NO_2 substitution (scheme 1).

Heterocyclic imidazole derivatives have attracted significant consideration because of their unique optical properties and play a main role in chemistry as an intermediary for synthetic reactions.[6] Imidazole nucleus forms the primary structure of several well-known biomolecules and also has considerable analytical applications by virtue of their chemiluminescence and fluorescence.[7] Aromatic nitro compounds and their derivatives are used as analytical reagents, solvents, and are important intermediates in the organic synthesis of explosives, pesticides, drugs, and perfumes.[8,9]

With continued shrinking of the size of conventional silicon-based electronics, molecular electronics has been proposed to be the future nanoscale electronic devices.[10] Recently, many potentially applicable molecular electronic devices, like molecular switches, field-effect transistors, wires and rectifiers devices have been investigated.[11] A wide range of molecular switches has been presented in the literature, activated with different kinds of external motive.[12] Light is a marvelous stimulus because its fast response time. In the present work, Non-equilibrium Green's function (NEGF) formalism combined with first-principles density functional theory (DFT) were used to investigate molecular conductance of the title compound.

Ab initio quantum-mechanical method is at present widely used for simulating IR spectrum and studying isomeric compounds.[13–17] In this study, vibrational spectra, optimized geometry, electronic absorption spectra, reactivity descriptors, molecular electrostatic potential and the electron transport properties of the title compound have been studied.

*For correspondence

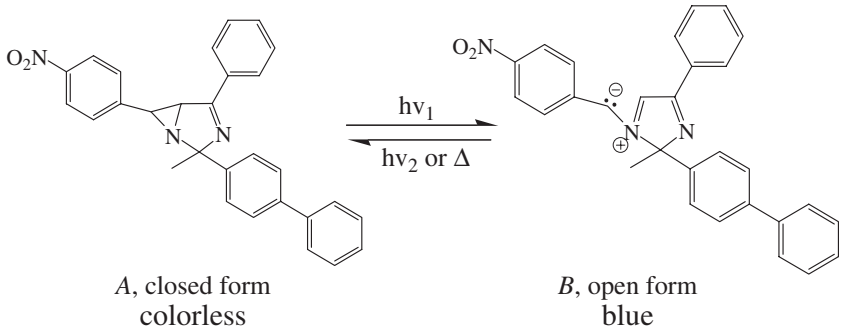

Scheme 1. Structures and Photochromic reaction of the title compound.

2. Experimental

2.1 *Materials and measurements*

The mid-IR spectra were obtained in the 4000–400 cm^{-1} region with a spectral resolution of 2 cm^{-1} by averaging the results of 10 scans with a Perkin-Elmer RXI Fourier Transform spectrophotometer using KBr pellet technique. The ultraviolet absorption spectra were recorded in the range 200–800 nm using Perkin-Elmer lambda 25 recording spectrophotometer equipped with a 10 mm quartz cell. The photoinduced form was formed upon UV irradiation (Hg lamp DRSh-260+ UV-transmitting glass filters). The NMR spectrum was recorded for the title compound at the ambient temperature on a Brucker AVANCE DRX 400 MHz using $CDCl_3$ as a solvent. All the chemicals and reagents were purchased from Merck and Fluka and were used without further purification. The development of the reaction was checked by thin layer chromatography (TLC) analysis on silica gel 60 GF_{254} aluminum sheets, using ethyl acetate: petroleum ether (1: 3) as the mobile phase. The spots were exposed to UV light and iodine vapor.

Synthesis of the 2-([1,1'-biphenyl]-4-yl)-2-methyl-6-(4-nitrophenyl)-4-phenyl-1,3 diazabicyclo [3.1.0]hex-3-ene is explained in Supplementary Information.

2.2 *Computational methods*

The calculations for the title compound have been done with a hybrid functional B3LYP at 6-311G(d,p) and basis set. All the calculations were performed using G03 program package.[18] The molecular structure of the title compound in the ground state was optimized. For all the calculations for this study, optimized structural parameters were used. The vibrational frequencies were calculated and scaled.[19] The Lorentzian function has been employed for deconvolution of IR spectrum using the Genplot package. ^{1}H NMR chemical shifts were calculated using the standard GIAO/DFT (Gauge-Independent Atomic Orbital).[20] Electronic excitations of the title compound were calculated by using TD-DFT in the gas phase.[21]

The transport properties of the molecular junction were calculated using the TranSIESTA package[22] which is based on the combination of DFT with the nonequilibrium Green's function (NEGF) technique. In NEGF theory, the molecular wire junction is separated into three regions: left electrode (L), contact region (C), and right electrode (R). In the lateral dimension, a 6×6 supercell was used, large enough to remove interactions between periodic images. Based on previous issues about self-assembled monolayers (SAMs), it is accepted that hydrogen atoms are dissociated upon adsorption to metal surfaces.[23] So, the two terminal hydrogen atoms bonded to the sulfur atoms are omitted from the optimized structure, and the remaining segment is put between two parallel Au(111) surfaces, which have a face-centered cubic (f.c.c.) lattice.

The structural optimization is accomplished in the SIESTA package[24] with the maximum force of 0.02 eV/Å, and core electrons are modeled using Troullier-Martins[25] soft norm-conserving pseudopotentials. The Perdew–Burke–Ernzerhof (PBE) exchange–correlation functional was adopted for the generated gradient approximation (GGA).[26] There is a good compromise of prior theoretical simulations with experimental measurements.[27] The Au atoms are described as a single-ξ plus single polarization (SZP) basis set while for the other atoms a double-ξ plus single polarization (DZP) basis set is used. The current through the device is computed using the Landauer–Büttiker formula in the TranSIESTA package.[22]

$$I = \frac{2e}{h} \int T(E, V)[f(E - \mu_L) - f(E - \mu_R)]dE \quad (1)$$

Here, e is the electron charge, h Planck's constant, $T(E, V)$ the transmission function at energy E under bias voltage V, and $f(E - \mu_{L(R)})$ is the Fermi–Dirac

distribution function with the electrochemical potential $\mu_{L(R)}$ of the left (right) electrode.

3. Results and Discussion

3.1 *Geometrical parameters*

The optimized geometrical parameters of the title compound were calculated by using DFT/B3LYP method with 6-311G(d,p) basis set which are listed in table S1 in accordance with numbering scheme given in figure 1. Some selected geometric parameters (Å, °) of "A" and "B" forms are presented in table 1. The optimized structure may be contrasted with other similar systems for which the crystal structures have been solved. Since the identification of all the normal modes of vibration of large molecules is not explicit, we tried to streamline the problem by considering each molecule as substituted benzene as this idea has been used several times in the past.[28] In the following discussion,

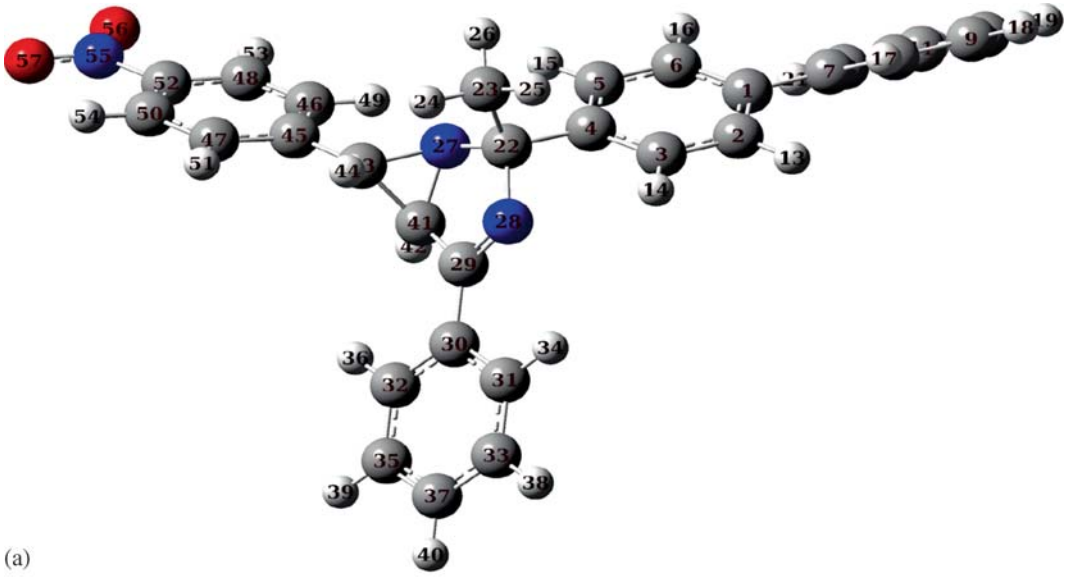

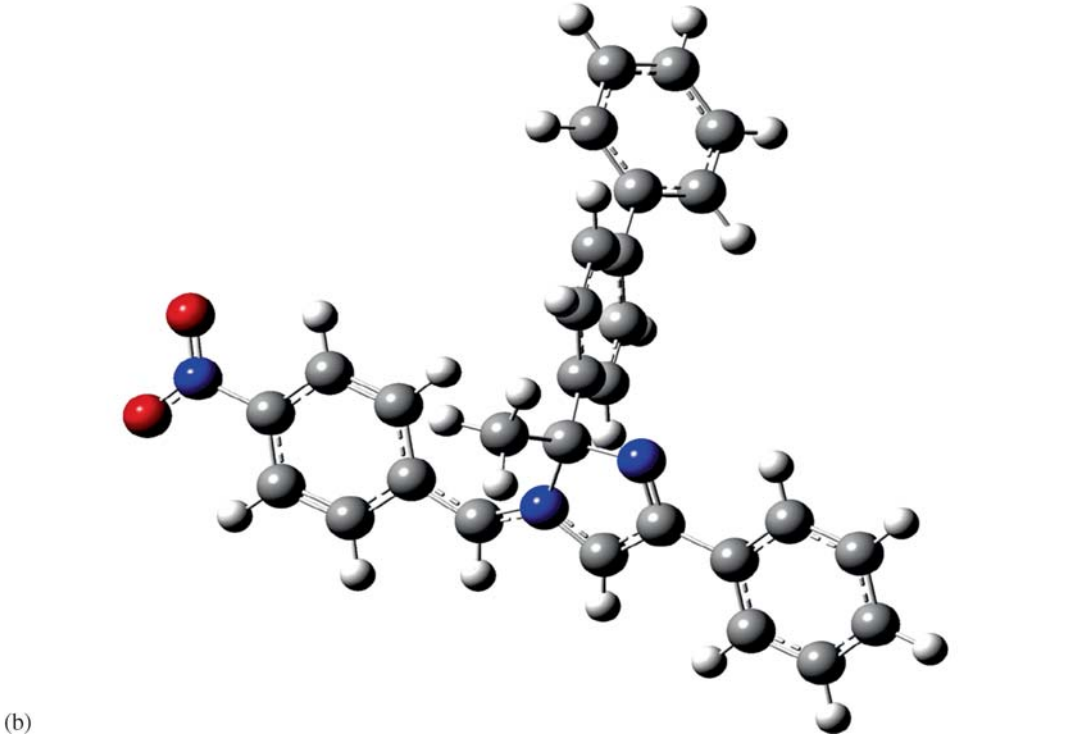

Figure 1. Optimized geometry by B3LYP/6-311++G(d,p) for (a) "A" and (b) "B" forms.

Table 1. Selected geometric parameters of "A" and "B" forms, atom labeling according to figure 1.

Parameters	"A"	"B"		"A"	"B"
Bond lengths (Å)			Bond lengths (Å)		
C_4-C_{22}	1.5347	1.5319	N_{27}-C_{41}	1.4612	1.0790
C_{22}-C_{23}	1.5361	1.5361	C_{41}-H_{42}	1.0870	1.3530
C_{23}-H_{24}	1.0933	1.0923	N_{27}-C_{43}	1.4665	1.3465
C_{22}-N_{28}	1.4759	1.3079	C_{43}-H_{44}	1.0888	1.0858
N_{28}-C_{29}	1.2850	1.4767	C_{43}-C_{45}	1.4899	1.4349
C_{29}-C_{30}	1.4721	1.4027			
Bond angles (°)			Bond angles (°)		
A(4, 22, 23)	109.6	116.7	A(22, 27, 41)	105.0	105.3
A(22, 23, 24)	111.7	108.5	A(27, 41, 42)	119.3	121.3
A(22, 23, 25)	109.4	109.3	A(22, 27, 43)	116.0	130.6
A(22, 23, 26)	109.9	112.6	A(27, 43, 44)	118.4	111.5
A(4, 22, 27)	108.7	110.7	A(27, 43, 45)	117.6	134.0
A(4, 22, 28)	109.0	107.9	A(43, 45, 46)	121.5	128.6
A(22, 28, 29)	109.2	108.0	A(43, 45, 47)	119.4	114.8
A(28, 29, 30)	123.7	122.1			
Dihedral angles (°)			Dihedral angles (°)		
D(3, 4, 22, 23)	84.8	35.0	D(28, 29, 30, 31)	−9.8	−6.0
D(4, 22, 23, 24)	−176.8	−179.6	D(28, 29, 30, 32)	169.8	−179.9
D(4, 22, 23, 25)	−57.1	−62.5	D(4, 22, 27, 41)	111.3	115.2
D(4, 22, 23, 26)	62.0	59.5	D(4, 22, 27, 43)	177.2	−68.3
D(3, 4, 22, 27)	−153.0	−87.5	D(22, 27, 43, 44)	8.8	−173.1
D(3, 4, 22, 28)	−36.4	−87.5	D(22, 27, 43, 45)	153.3	4.7
D(4, 22, 28, 29)	−110.8	−117.4	D(27, 43, 45, 46)	14.5	15.9
D(22, 28, 29, 30)	176.8	179.3	D(27, 43, 45, 47)	−166.8	−166.1

the nitrobenzene, benzene, and biphenyl are assigned as PhI, PhII and PhIII, respectively, and the 4-methyl-3,5-diaza-bicycle [3.1.0]hex-2-ene as Ring. For "B" form, PhI, PhII and PhIII are similar and 1,2-dimethyl-2,5-dihydro-1H-imidazole is assigned Ring.

Dhanabal *et al.*,[29] reported the N-O and C-N bond lengths in the range of 1.198–1.238 and 1.440–1.525 Å. Sundaraganesan *et al.*,[30] stated C-N and N-O bond lengths as 1.453, 1.460 Å and in the range 1.273–1.275 Å, respectively. For "A" form, the N-O bond lengths are 1.231 Å and C-N bond lengths are 1.461–1.502 Å, and for "B" form, N-O and C-N bond lengths are in the range 1.236–1.236 Å and 1.347–1.553 Å, respectively, which are in agreement with the reported values. The CNO angles are reported[33] in the range 117.4–118.7°, whereas for the "A" form it is 117.7° and for "B" form it is 117.9–118.0°. Sridevi *et al.*,[31] reported N = C, N_{28}-C_{22} bond lengths and O-N-O, O-N-C bond angles as 1.283, 1.357 Å and 125.3, 118.0–116.6° for 5-chloro-1-methyl-4-nitro-1H-imidazole. In the present case, for "A" form the respective bond lengths are 1.285, 1.476 Å and bond angles 124.6, 117.7, and for "B" form bond lengths are 1.308, 1.448 Å and bond angles are 124.2, 117.9–118.0°.

The Global minimum energies obtained for dimer were −2867.13672 and −2867.11578 Hartrees by DFT method and the corrected intermolecular energies were −2867.13486 and −2867.11399 Hartrees in BSSE method for "A" and "B" forms, respectively. The energy differences were only 0.0018621 and 0.0017914 Hartrees confirming that in the present case this method seemed to be compatible.

3.2 *Vibrational analysis*

The title compound contains 57 atoms, and it has 165 normal modes of vibration. The assignments of the observed infrared vibrational bands have been performed and compared with the calculated frequencies. The calculated wavenumbers are generally scaled by scaling factor to evaluate with observed wavenumbers.[15] The experimental FT-IR spectrum of the title compound in the region 4000–400 cm^{-1} is shown in figure 2. For obvious identification of these bands, we used band deconvolution techniques in the IR spectrum. A deconvoluted IR spectrum of the title compound is shown in figure S1 (Supplementary Information). The observed IR bands and calculated wavenumbers (scaled) and assignments are given in table S2

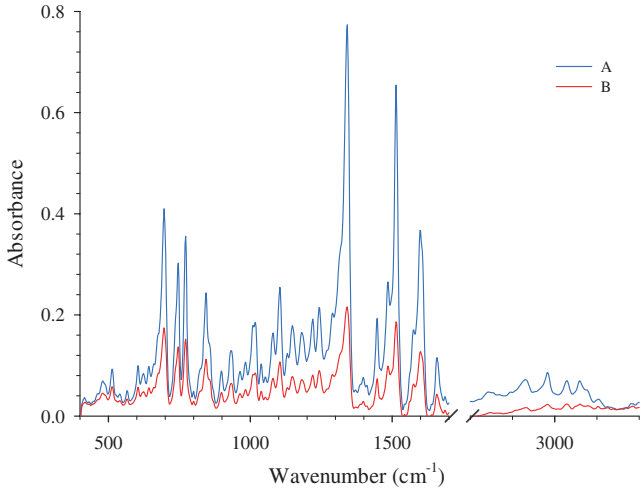

Figure 2. FT-IR spectra (experimental) for "A", before irradiation; and "B", after irradiation for 50 s at 300 nm.

(Supplementary Information). The correlation diagram for the calculated and the experimental frequencies of "A" and "B" forms are shown in figure S2 (Supplementary Information).

The connection between the calculated and experimental wavenumbers is linear and described by the following equations:

$$\text{For "A" form:} \quad \upsilon_{\text{cal.}} = 0.9864\upsilon_{\text{exp.}} + 8.4408 \quad (R^2 = 0.9978) \qquad (2)$$

$$\text{For "B" form:} \quad \upsilon_{\text{cal.}} = 0.9874\upsilon_{\text{exp.}} + 0.5383 \quad (R^2 = 0.9983) \qquad (3)$$

Aromatic nitro compounds displayed strong absorption due to the asymmetric and symmetric vibrations of the NO_2 group in 1570–1485 cm^{-1} and 1370–1320 cm^{-1}, respectively.[32] Deconvoluted IR spectra of "A" form showed the presence of two bands observed to the asymmetric vibrations of the NO_2 group in 1602, 1498 cm^{-1} (see figure S1a in Supplementary Information) and in 1603, 1552 cm^{-1} (B3LYP). The symmetric stretching mode for "A" form was observed at 1348 cm^{-1} in FT-IR which coincides with the theoretically computed value 1342 cm^{-1}.

The NO_2 scissors[33] appear at higher wavenumbers (850 ± 60 cm^{-1}) when conjugated to C-C or aromatic molecules. For nitrobenzene, δNO_2 is reported[26] at 852 cm^{-1}. Deconvoluted IR spectra for "A" form indicated the presence of two bands at 852 and 774 cm^{-1} in the IR spectrum and 848 and 819 cm^{-1} in B3LYP are assigned as δNO_2 modes. In aromatic compounds, the wagging mode ωNO_2 is expected in the region 740 ± 50 cm^{-1} with a moderate to strong intensity, a region in which γCH is also active.[26] Deconvoluted IR spectra for "A" form indicates the presence of two bands at 738 and 644 cm^{-1} in the IR spectrum, and 725 and 680 cm^{-1} in B3LYP calculation that belong to γNO_2 modes. The rocking mode, ρNO_2 is active in the region 540 ± 70 cm^{-1} in aromatic nitro compounds.[26] For "A" form, the FT-IR band observed at 512 cm^{-1} corresponds to ρNO_2 rocking vibration while theoretically computed value was 516 cm^{-1}. Suryanarayana *et al.*,[34] reported the range 65 ± 10 cm^{-1} as the τNO_2 for aromatic compounds. In the "A" form, the deformation modes of NO_2 are assigned at 65 and 27 cm^{-1} (B3LYP).

The C=N stretching skeletal bands are expected in the 1585 cm^{-1}.[35] Deconvoluted IR spectra of "A" form showed the appearance of two bands in 1664, 1578 cm^{-1} in IR spectrum. The identification of the C–N vibration is a very difficult task since mixing of several bands is possible in this region. Melardi *et al.*,[36] assigned the C–N stretching absorption in 1305 cm^{-1} for aromatic amines. In "A" form, the theoretical calculation gives 1364, 1324 and 1231 cm^{-1} as C-N stretching modes matching with bands at 1398, 1334 and 1224 cm^{-1} in the IR spectrum.

The band at 2739 cm^{-1} is assigned to the CH_3 asymmetric stretching.[37] The C–H stretching in methyl group occurs at lower frequencies than the use of the aromatic ring (3100–3000 cm^{-1}). The B3LYP calculations give $\upsilon_a CH_3$ at 3031, 3022 and 3015 cm^{-1} and $\upsilon_s CH_3$ at 2944 cm^{-1}. The bands at 2895 and 2845 cm^{-1} in IR spectrum are assigned as $\upsilon_a CH_3$ and $\upsilon_s CH_3$ for the "A" form. For the "A" form, the scissoring mode of the CH_3 group is assigned at 1449, 1440, 1364 and 1360 cm^{-1} (B3LYP) and 1446, 1398 cm^{-1} (IR). In "A" form, the CH_3 wagging mode is observed at 1110, 1072 cm^{-1} and in the IR spectrum at 1212, 1120, 1110, 1088 and 1062 cm^{-1} theoretically. The rocking vibrations of the CH_3 group are generally observed in the region 1070–1010 cm^{-1}.[37] The band at 926 cm^{-1} in the IR spectrum and at 918, 908, 882 and 871 cm^{-1}(B3LYP) are assigned as ρCH_3 mode for the "A" form. The bands at 259, 238, 221 and 206 cm^{-1} (B3LYP) are assigned as the twisting mode τCH_3.

Sajan *et al.*,[38] assigned the C–H stretching vibrations absorption in the region 3064–3012 cm^{-1} for aromatic amines. In "A" form the bands observed at 3182, 3103, 3079, 3060, 3028, 2982 and 2929 cm^{-1} in the IR spectrum are assigned to the C-H stretching modes of the phenyl rings. The B3LYP calculations give these modes in the range 3048–3086 cm^{-1}.

The C-H out-of-plane deformations of γCH is observed between 1000 and 700 cm^{-1}.[33,34] The aromatic C–H in-plane bending modes of benzene and its derivatives are observed in the region 1300–1000 cm^{-1}. The C–H out-of-plane bending modes, usually of medium intensity, arise in the region 950–600 cm^{-1}.[39]

In the case of "A" form, the bands observed at 1334, 1244, 1180, 1142, 1096, 1012 cm^{-1} are assigned to the C-H in-plane bending modes of the phenyl rings. The aromatic C–H out-of-plane bending vibrations of the title compound is assigned to the medium to weak bands observed at 926, 754, 692, 600, 560 cm^{-1} for "A" form in the infrared spectrum.

The IR frequency regions for the "B" form are similar to "A" form.

3.3 ^{1}*H NMR spectrum*

The ^{1}H spectrum of the title compound in "A" form was recorded in $CDCl_3$ (figure 3). The ^{1}H NMR theoretical chemical shifts and the assignments of the title compound are presented in table S3 (Supplementary Information), according to atom numbering in the figure 1. The geometry of the title compound, together with that of tetramethylsilane (TMS), is fully optimized. Then, ^{1}H chemical shift calculation of the compound was done by the same method using 6-311G(d,p) basis set IEFPCM/chloroform solution.[20] The chemical shifts of the aliphatic proton appeared in the high field while aromatic protons of organic compounds are usually seen in the range of 7.00–8.00 ppm. The signals of the eighteen aromatic protons (^{1}H) of the title compound were calculated theoretically as 7.37–8.61 ppm and experimentally observed at 7.27–8.28 ppm. We predicted H_{19} at 7.37 ppm in the lower field and H_{54} at 8.61 ppm in the highest field of the aromatic region. It could be seen from table S3 that chemical shifts that is obtained through theory are in agreement with the experimental NMR data.

3.4 *Molecular electrostatic potential (MEP) surface*

Molecular electrostatic potential (MEP) is used for comparative reactivities towards electrophilic attack and nucleophilic reactions.[40] To predict reactive sites for electrophilic and nucleophilic attack for "A" and "B" forms, the MEP at the B3LYP/6-311G(d,p) method was calculated. The negative (red and yellow) and the positive (blue) regions of MEP were related to electrophilic and nucleophilic reactivities are shown in figure S3 (Supplementary Information) where blue shows the strongest attraction and red shows the strongest repulsion. MEP color scale is such that $\delta^+ \rightarrow \delta^-$ in the direction red $\rightarrow$ blue. The maximum negative electrostatic potential is prominent over O_{56} and O_{57} atoms. The maximum negative electrostatic potential value for these electrophilic sites calculated at B3LYP/6-311G(d,p) are about $-22.339(O_{56})$, $-22.340(O_{56})$ and $-22.371(O_{56})$, $-22.371(O_{56})$ a.u. for "A" and "B" forms. The fitting point charges to those electrostatic potentials are $-0.443(O_{56})$, $-0.451(O_{57})$ and $-0.437(O_{56})$, $-0.440(O_{57})$. For the feasible nucleophilic reaction, the maximum positive region is located on hydrogen bond to C atoms. The higher

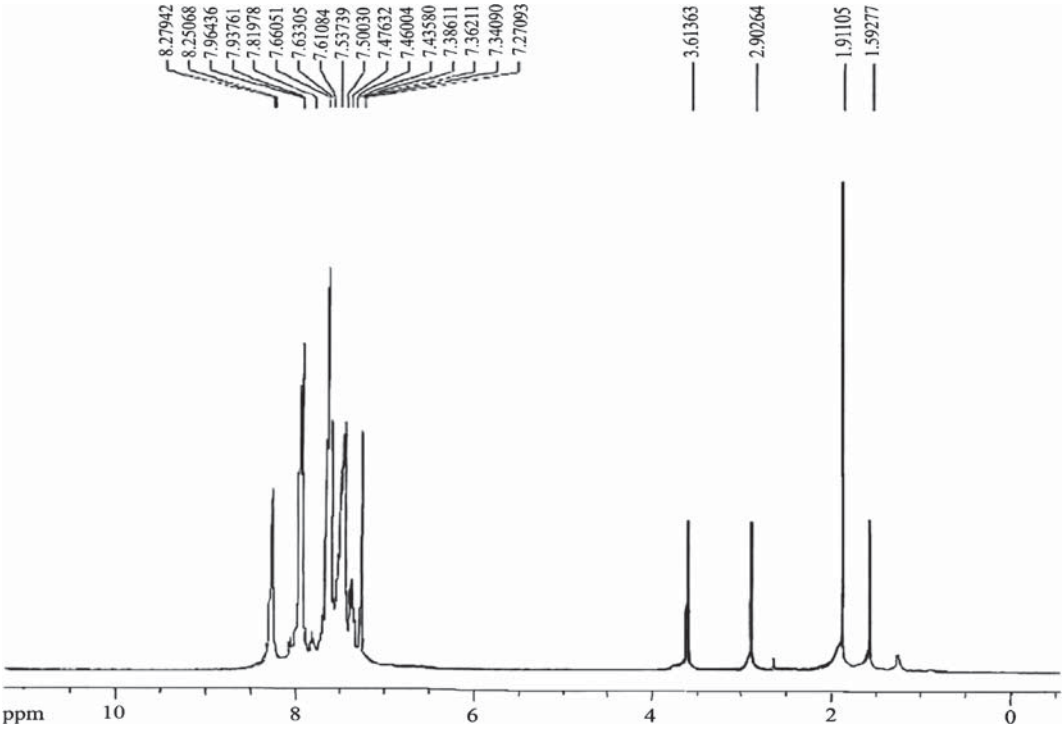

Figure 3. ^{1}H NMR (400.224 MHz, $CDCl_3$) spectrum of "A" form at 294.8 K.

electronegativity in the nitro group makes it the most reactive part of the molecule.

3.5 *HOMO–LUMO band gap*

Gauss-Sum 2.2 Program[41] was used to calculate group contributions to the molecular orbitals (HOMO and LUMO) and provide the density of the state (DOS) as shown in figure S4 (Supplementary Information). DOS plot shows population analysis per orbital and indicates an easy outlook of the makeup of the molecular orbitals in a certain energy range. The energy split between the HOMOs and LUMOs are the critical parameters in special molecular electrical transport properties which help in the measure of electron conductivity.[42] The HOMO represents the ability to donate an electron whereas LUMO represents the ability to obtain the electron. The energy difference between the HOMO and LUMO illustrate the charge conduction interaction within the molecule The frontier orbital gaps in the case of "A" and "B" forms were found to be 3.592 eV and 2.397 eV, respectively, obtained by TD-DFT method using 6-311G(d,p) basis set in the gas phase (see figure S5 in Supplementary Information). The conjugated molecules are noted for low HOMO–LUMO separation. Therefore, an electron density conduction happens from the maximum aromatic region of the π-conjugated system in the electron-donor side to its electron-withdrawing part. Upon excitation, intramolecular electron displacement occurs from the phenyl group to the nitrobenzene moiety, where phenyl and nitrobenzene groups acted as electron donor and acceptor, respectively.

3.6 *Electronic spectra*

Experimentally observed UV–Vis absorption spectra of "A" and "B" forms recorded in ethanol solvent are presented in figure 4.

The first excited state of open form has been fully optimized based on the optimized ground state geometric conformation as the initial conformation with the TDDFT method.[21] The calculated absorption spectra in this work are for the first 10 singlet excited states and all the calculated emission spectra are for the first 6 low lying singlet excited states. Based on the TDDFT/B3LYP/6-311G(d,p) calculated level, the corresponding absorption and fluorescence spectra of open form are displayed in figure S6 (Supplementary Information). It should be noted that the strong absorption peak for open form is located at 430 nm (23256 cm^{-1}) (listed in table 2), which is in

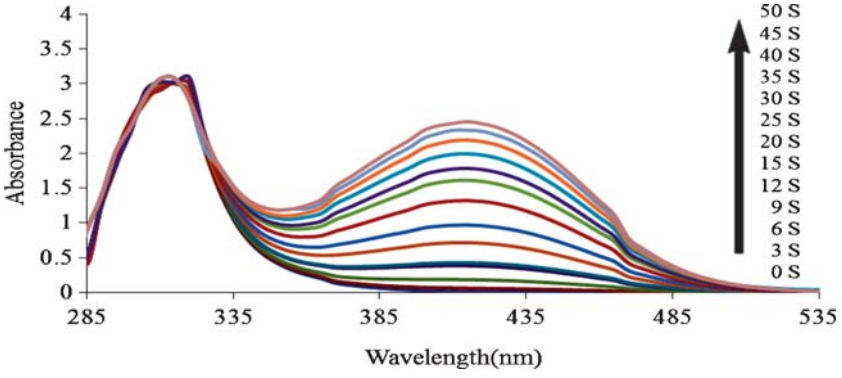

Figure 4. UV-Vis absorption spectra of the title compound upon irradiation under 300 nm light in EtOH at a concentration of 2×10^{-3} M with a 10 mm quartz cell before and after successive UV irradiation ($\lambda_{max} = 310$ nm for "A" and 310, 415 nm for "B").

Table 2. Experimental and calculated absorption wavelength and oscillator strengths of "A" and "B" forms using the TD-DFT method at the B3LYP/6-311G(d,p) level.

	Ethanol		Gas		Exp.		
Comp.	λ (nm)	*f*	λ (nm)	*f*	λ (nm)	Assignment	[a]Gas major contribution
"A"	310.3	0.085	318.6	0.136	310	$\pi \rightarrow \pi^*$	H→L(75%), H-2→L+1(21%)
"B"	315.8	0.070	318.4	0.089	310	$\pi \rightarrow \pi^*$	H-1→L(91%)
	430.2	0.848	443.8	0.663	**415**	n→ π^*	H→L(98%)

[a]H: HOMO, L: LUMO

consistent with 24096 cm^{-1} (415 nm) in the experiment. The results of open form shown in figure S6 reveal a normal Stokes shifted emission maximum at 546 nm (18315 cm^{-1}) in ethanol.

For both "A" and "B" forms of the title compound, wavelength (λ), oscillator strength (f) and major contributions of calculated transitions are given in table 2. The calculated excitation energies of the transition are compared with the experimental values and the results are in good agreement.[15]

The UV–Vis band in "A" form is observed at 310 nm (colorless), and for "B" form bands are observed at 310, 415 nm (blue color) due to the formation of zwitterionic doubly charged imine ylide (open form). The observed band at 310 nm is due to the $\pi \rightarrow \pi^*$ transition. The more important band observed at 415 nm for "*B*" form belong to the dipole-allowed n$\rightarrow$ π^* transition. "B" form was also converted to "A" form after being held at 90°C for 4–5 min.

The results of TD-DFT show an appreciable red-shift in solvent and the degree of red-shift in vacuum is more significant than that in solvent. The discrepancy between vacuum and solvent effects in TD-DFT calculations may result from two aspects. The first aspect is that smaller gap of materials which induces smaller excited energies. The other is solvent effects. Experimental measurements of electronic absorption are usually performed in solution. Solvent, especially in polar solvent, could affect the geometry and electronic structure as well as the properties of molecules through the long-range interaction between solute and solvent molecules.

The HOMO-LUMO gap of the title compound in ethanol (3.659 and 2.552 eV for "A" and "B" forms) at TD-DFT/B3LYP/6-311G(d,p) theory level is bigger than that in vacuum (3.5918 and 2.3962 eV for "A" and "B" forms). A general hypochromic shift (blue shift) was noticed from the gas phase to the polar solvent ethanol. We propose that these observations are due to the role of the nitrogen dioxide (NO_2) functionality which induces charge- transfer and intermolecular hydrogen bonding. The observed blue shift can be described by the hydrogen acceptor ability of the organic molecule and the hydrogen donor ability of the relevant solvents.[43] This fact designates that the solvent effects destabilize the frontier orbitals of the title compound. Hence, it induces blue-shift of the absorption as compared with that in vacuum.

3.7 *Global reactivity parameters*

The energies of frontier molecular orbitals (E_{HOMO}, E_{LUMO}), energy band gap (E_{HOMO}- E_{LUMO}), electronic chemical potential (μ), electronegativity (χ), global hardness (η), global softness (S), and electrophilicity indices (ω) have been listed in table 3, which were calculated on the basis of E_{HOMO} and E_{LUMO}, using the following equations.[44]

$$\mu = \frac{1}{2}\left(E_{LUMO} + E_{HOMO}\right) \tag{4}$$

$$\chi = -\mu = -\frac{1}{2}\left(E_{LUMO} + E_{HOMO}\right) \tag{5}$$

$$\eta = \frac{1}{2}\left(E_{LUMO} - E_{HOMO}\right) \tag{6}$$

$$S = \frac{1}{2\eta} \tag{7}$$

$$\omega = \frac{\mu^2}{2\eta} \tag{8}$$

Table 3. Calculated energy values of "A" and "B" forms by B3LYP/6-311G(d,p) basis set.

Chemical parameters	"A" form	"B" form
E_{HOMO} (eV)	−6.0089	−4.9426
E_{HOMO-1} (eV)	−6.6745	−6.2680
E_{LUMO} (eV)	−2.4171	−2.5464
E_{LUMO+1} (eV)	−1.5896	−1.4212
$E_{HOMO-LUMO}$ gap (eV)	3.5918	2.3962
Chemical potential (μ)	−4.2130	−3.7445
Global hardness (η)	1.7959	1.1981
Global softness (S)	0.2784	0.4173
Elecronegativity (χ)	4.2130	3.7445
Electrophilicity index (ω)	4.9416	5.8515

Electrophilicity index is one of the main quantum chemical descriptors in characterizing biological or toxicity activities of the molecules in the background of expansion of Quantitative Structure Activity Relationship (QSAR) parlance.[45] The computed electrophilicity index of the title compound also describes the biological activity of drug-receptor interaction.

3.8 *Current–Voltage Characteristics of Linear Molecular Switches*

As illustrated in figure S7 (Supplementary Information), the molecular electronic device is divided into several regions: the right electrode, the central scattering region, and the left electrode. Figure 5 shows the calculated I–V characteristics of the system for the two forms at a bias up to 2 V. It should be noted that at each bias, the current is determined self-consistently under the nonequilibrium condition. The switching action can be obviously seen in figure 5; the current of open ("B") form is greater than that of closed ("A") form at the same bias. It can be concluded that there is a switch from *on* (low resistance) state to the *off* (high resistance) state when the open form of the molecule changes to the closed form.

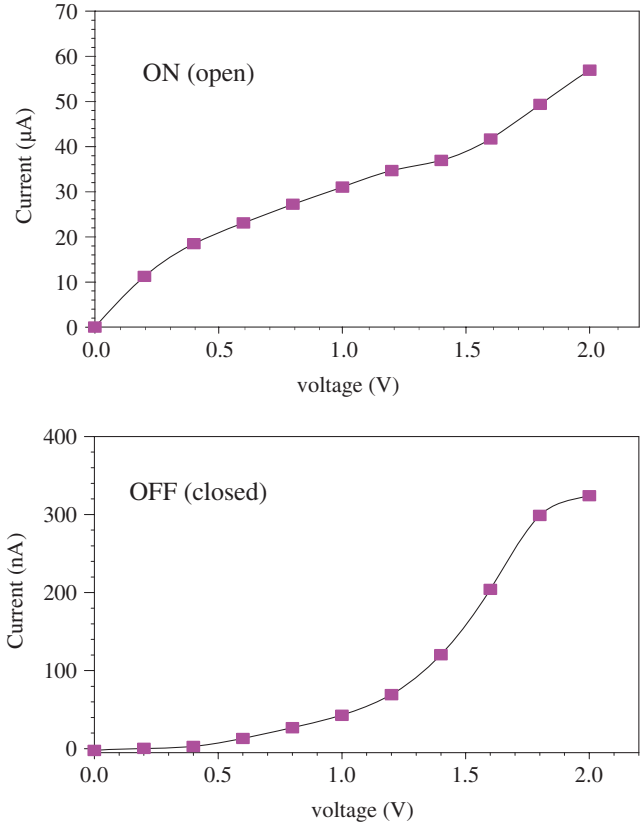

Figure 5. Calculated current−voltage (I–V) characteristics for OFF and ON state structures, 'A' and 'B' forms, of the title compound. Note the different scales for the calculated currents in the ON and OFF state.

As shown in Landauer–Bütiker formula (Eq. 1), calculated values for the current for the system is dependent on the transmission spectra. The switching behavior of this compound can be perceived from the energy affiliation of zero bias transmission spectra, which are shown in figure S8 (Supplementary Information). In our computation, the average Fermi level is set as zero. From Eq. 1, we can expect that only electrons with energies within a range close the Fermi level E_F contribute to the total current. Therefore, a good approximation of the range of the bias window, i.e., [−V/2, +V/2] is adequate to analyze a finite section of the transmission spectrum.

It is clear in figure S8 that the transmission spectra of two isomers display tangibly disparate characteristics. When the system is with open form, the value of the transmission coefficient is smaller than that of closed form in the energy window of [−2.0, 2.0 eV]. Meanwhile, the HOMO and LUMO levels are −1.131, 0.169 eV for the open form and −1.943, 0.0.063 eV for the closed form. So, the HOMO–LUMO gap of the open form is smaller than that of the closed form. As a result, the absence of intense peaks in the window of [−2.0, 2.0 eV] and larger HOMO–LUMO gap because of the molecular structure of closed form account for its low conductivity.

4. Conclusions

The novel compound the 2-([1,1'-biphenyl]-4-yl)-2-methyl-6-(4-nitrophenyl)-4-phenyl-1,3 diazabicyclo [3.1.0]hex-3-ene was synthesized for the first time and characterized by IR, UV–Vis and NMR. The entire calculations for the title compound were done with a hybrid functional B3LYP at 6-311G(d,p) and basis set. The UV–Vis band in "A" (closed) form is observed at 310 nm (colorless), and for "B" (open) form at 310 and 415 nm (blue color) due to the formation of zwitterionic doubly charged imine ylide (open form). Also, molecular electrostatic potential map (MEP), frontier molecular orbital analysis (HOMO–LUMO), total density of state (TDOS) and reactivity descriptors were found and discussed.

Title compound has been proposed as a potential molecular switch for electronic device, in particular, a photoinduced molecular switch. This molecule has two stable conformations (closed and open) in its ground state, which makes it a promising component of molecular devices, and can be converted from one conformation to the other by photoexcitation. The open form

("B") has a conductance considerably higher than that of the closed form ("A") at equilibrium (zero bias), enabling its use as a molecular switch with ON and OFF states.

Supplementary Information (SI)

All additional information pertaining to synthesis of the title compound, deconvoluted IR spectra (figure S1), correlation between the calculated and the experimental frequencies (figure S2), molecular electrostatic potential surface (figure S3), TDOS diagrams (figure S4), frontier molecular orbital (figure S5), calculated absorption and fluorescence spectra of open form (figure S6), schematic molecular junctions (figure S7), transmission spectra of the molecular switch at zero bias (figure S8), characterization of the geometry optimization of "*A*" and "*B*" forms (table S1), observed and calculated (scaled) selected frequencies (cm^{-1}) for "*A*" and "*B*" forms (table S2), experimental and theoretical ^1H NMR isotropic chemical shifts (table S3), are given in the Supporting Information, available at www.ias.ac.in/chemsci.

Acknowledgments

The authors are grateful to Dr. Mohammad Vakili (Ferdowsi University of Mashhad) for his kind assistance and help. Financial support of Damghan University is gratefully acknowledged.

References

1. Bousas-Laurent H and Durr H 2001 *Pure Appl. Chem.* **73** 639
2. Tighadouini S, Radi S, Toupet L, Sirajuddin M, Ben Hadda T, Akkurt M, Warad I, Mabkhot Y N and Ali S 2015 *J. Chem. Sci.* **127** 2211
3. Chen Y, Pang M L, Cheng K G, Wang Y, Han J, He Z J and Meng J B 2007 *Tetrahedron* **63** 4319
4. Mahmoodi N O, Tabatabaeian K and Kiyani H 2012 *Helv. Chim. Acta* **95** 536
5. Mahmoodi N O and Kiyani H 2004 *Bull. Korean Chem. Soc.* **25** 1417
6. Kamidate T, Yamaguchi K and Segawa T 1989 *Anal. Sci.* **5** 429
7. Ucucu U, Karaburun N G and Isikdag I 2001 *IL Farmaco* **56** 285
8. Eaton D F 1991 *Science* **253** 281
9. Becker F F and Banik B K 1998 *Bioorg. Med. Chem.* **50** 2877
10. Joachim C, Gimzewski J K and Aviram A 2000 *Nature* **408** 541
11. Poulsen K M and Bjørnholm T 2009 *Nat. Nanotechnol.* **4** 551
12. Galperin M and Nitzan A 2012 *Phys. Chem. Chem. Phys.* **14** 9421
13. Vakili M, Tayyari S F, Kanaani A, Nekoei A R, Salemi S, Miremad H, Berenji A R and Sammelson R E *J. Mol. Struct.* **998** 99
14. Vakili M, Nekoei A R, Tayyari S F, Kanaani A and Sanatid N 2012 *J. Mol. Struct.* **1021** 102
15. Kanaani A, Ajloo D, Kiyani H and Farahani M 2014 *J. Mol. Struct.* **1063** 30
16. Kanaani A, Ajloo D, Ghasemian H, Kiyani H, Vakili M and Mosallanezhad A 2015 *Struct. Chem.* **26** 1095
17. Kiyani H, Kanaani A, Ajloo D, Ghorbani F and Vakili M 2014 *Res. Chem. Intermed.* **41** 7739
18. Frisch M J, Trucks G W, Schlegel H B, Scuseria G E, Robb M A, Cheeseman J R, Scalmani G, Barone V, Mennucci B, Petersson G A, Nakatsuji H, Caricato M, Li X, Hratchian H P, Izmaylov A F, Bloino J, Zheng G, Sonnenberg J L, Hada M, Ehara M, Toyota K, Fukuda R, Hasegawa J, Ishida M, Nakajima T, Honda Y, Kitao O, Nakai H, Vreven T, Montgomery J A Jr, Peralta J E, Ogliaro F, Bearpark M, Heyd J J, Brothers E, Kudin K N, Staroverov V N, Keith T, Kobayashi R, Normand J, Raghavachari K, Rendell A, Burant J C, Iyengar S S, Tomasi J, Cossi M, Rega N, Millam J M, Klene M, Knox J E, Cross J B, Bakken V, Adamo C, Jaramillo J, Gomperts R, Stratmann RE, Yazyev O, Austin A J, Cammi R, Pomelli C, Ochterski J W, Martin R L, Morokuma K, Zakrzewski V G, Voth G A, Salvador P, Dannenberg J J, Dapprich S, Daniels A D, Farkas O, Foresman J B, Ortiz J V, Cioslowski J, Fox D J 2004 Gaussian 03, Revision E.01 (Gaussian, Inc. : Wallingford)
19. Foresman J B 2000 In *Exploring Chemistry with Electronic Structure Methods: A Guide to Using Gaussian* (Pittsburg: Gaussian Inc)
20. Wolinski K, Hinton J F and Pulay P 1990 *J. Am. Chem. Soc.* **112** 8251
21. Casida M E, Casida K C and Salahub D R 1998 *Int. J. Quantum Chem.* **70** 933
22. Brandbyge M, Mozos J L, Ordejon P, Taylor J and Stokbro K 2002 *Phys. Rev. B* **65** 165401
23. Cao Y, Ge Q, Dyer D and Wang L 2003 *J. Phys. Chem. B* **107** 3803
24. Soler J M, Artacho E, Gale J D, García A, Junquera J, Ordejón P and Sánchez-Portal D J 2002 *J. Phys.: Condens. Matter* **14** 2745
25. Troullier N and Martins J L 1991 *Phys. Rev. B* **43** 1993
26. Perdew J P, Burke K and Ernzerhof M 1996 *Phys. Rev. Lett.* **77** 3865
27. Zhang G P, Hu G C, Li Z L and Wang C K 2012 *J. Phys. Chem. C* **116** 3773
28. Sett P, Chattopadhyay S and Mallick P K 2000 *Spectrochim. Acta A* **56** 855
29. Dhanabal T, Amirthaganesan G, Dhandapani M and Das S K 2012 *J. Chem. Sci.* **124** 951
30. Sundaraganesan N, Ayyappan S, Umamaheswari H and Joshua B D 2007 *Spectrochim. Acta A* **66** 17
31. Jensen J O, Banerjee A, Merrow C N, Zeroka D and Lochner J M 2000 *J. Mol. Struct. (THEOCHEM)* **531** 323
32. Kumar V and Balachandran V 2005 *Spectrochim. Acta A* **61** 1811
33. Roeges N P G 1994 In *A Guide to the Complete Interpretation of Infrared Spectra of Organic Structures* (New York: Wiley)

34. Suryanarayana V, Kumar A P, Rao G R and Panday G C 1992 *Spectrochim. Acta A* **48** 1481
35. Shinde Y, Sproules S, Kathawate L, Pal S, Konkimalla V B and Salunke-Gawali S 2014 *J. Chem. Sci.* **126** 213
36. Melardi M R, Shamsi Mogoll F B, Baball Sajirani A, Attar Gharamaleki J, Notash B and Rofouei M K 2015 *J. Chem. Sci.* **127** 2171
37. Gunasekaran S, Kumaresan S, Arunbalaji R, Anand G and Srinivasan S 2008 *J. Chem. Sci.* **120** 315
38. Sajan D, Jothy V B, Kurulvilla T and Joe I H 2010 *J. Chem. Sci.* **22** 511
39. El-Azhary A A 1999 *Spectrochim. Acta A* **55** 2437
40. Gunasekaran S, Balaji R A, Kumaresan S, Anand G and Srinivasan S 2008 *Can. J. Anal. Sci. Spectros.* **53** 149
41. N O'Boyle N M, Tenderholt A L and Langner K M 2008 *J. Comp. Chem.* **29** 839
42. Fukui K 1982 *Science* **218** 747
43. Kumar S, Sharma R, Kumar S and Nitika 2014 *Chem. Sci. Trans.* **3** 919
44. Padmanabhan J, Parthasarathi R, Subramanian V and Chattaraj P K 2007 *J. Phys. Chem. A* **111** 1358
45. Garrido A P, Helguera A M, Guillén A A, Cordeirom M N D S and Escudero A G 2009 *Bioorgan. Med. Chem.* **17** 896